





Intense ferromagnetic fluctuations preceding magnetoelastic first-order transitions in giant magnetocaloric $\text{LaFe}_{13-x}\text{Si}_x$

Zhao Zhang ^{1,2} Houbo Zhou,^{3,4} Richard Mole,⁵ Chenyang Yu,^{1,2} Zhe Zhang,^{1,2} Xinguo Zhao ¹ Weijun Ren,¹ Dehong Yu,^{5,*} Bing Li ^{1,2,†} Fengxia Hu,^{3,4,‡} Baogen Shen,^{3,4} and Zhidong Zhang ^{1,2}

¹Shenyang National Laboratory for Materials Science, Institute of Metal Research, Chinese Academy of Sciences, 72 Wenhua Road, Shenyang, Liaoning 110016, China

²School of Materials Science and Engineering, University of Science and Technology of China, 72 Wenhua Road, Shenyang, Liaoning 110016, China

³Beijing National Laboratory for Condensed Matter Physics and State Key Laboratory of Magnetism, Institute of Physics, Chinese Academy of Sciences, Beijing 100190, China

⁴School of Physical Sciences, University of Chinese Academy of Sciences, Beijing 100049, China

⁵Australian Nuclear Science and Technology Organisation, Locked Bag 2001, Kirrawee DC NSW 2232, Australia



(Received 7 May 2021; accepted 6 July 2021; published 22 July 2021)

First-order magnetic transitions are of both fundamental and technological interest given that a number of emergent phases and functionalities are thereby created. Of particular interest are giant magnetocaloric effects, which are attributed to first-order magnetic transitions and have attracted broad attention for solid-state refrigeration applications. While the conventional wisdom is that atomic lattices play an important role in first-order magnetic transitions, a coherent microscopic description of the lattice and spin degrees of freedom is still lacking. Here, we present a comparative neutron scattering study on the lattice and spin dynamics in intermetallic $\text{LaFe}_{11.6}\text{Si}_{1.4}$ and $\text{LaFe}_{11.2}\text{Si}_{1.8}$, which represent one of the most classical giant magnetocaloric systems and undergo first-order and second-order magnetic transitions, respectively. While their spin-phonon coupling effects are quite similar, $\text{LaFe}_{11.6}\text{Si}_{1.4}$ exhibits a much stronger magnetic diffuse scattering in the paramagnetic state preceding its first-order magnetic transition, corresponding to intense ferromagnetic fluctuations. These dynamic insights suggest that the magnetic degree of freedom dominates this magnetoelastic transition and ferromagnetic fluctuations might be universally relevant for this kind of compounds.

DOI: [10.1103/PhysRevMaterials.5.L071401](https://doi.org/10.1103/PhysRevMaterials.5.L071401)

I. INTRODUCTION

First-order magnetic transitions (FOMTs) take place with abrupt changes of several physical quantities at transition points with respect to temperature, magnetic field, electric field, pressure, stress, etc. [1–5]. Such features offer a great opportunity for applications in a variety of functional sensors with high intrinsic signal-to-noise ratios. More importantly, the multiple degrees of freedom are often strongly coupled at FOMTs so that some unprecedented functionalities become possible based on crossing control. FOMTs can be categorized into magnetostructural and magnetoelastic transitions [6]. The former involves two magnetic phases accommodating different crystallographic symmetries and are interpreted based on soft-mode phonons and their coupling with magnetic moments [7] and the lattice contribution to the entropy changes is crucial [8]. By contrast, there is a discontinuity of crystal unit cell volumes found in the latter with the crystallographic symmetry unchanged. The frequently adopted mechanism for this case is the itinerant electron metamagnetism (IEM) [9]. An

IEM transition, i.e., a FOMT from Pauli paramagnetic (PM) to ferromagnetic (FM) states in an itinerant magnetic system induced by external magnetic fields, is formulated based on the Landau-Ginzburg free energy expansion taking into account the renormalization effect associated with spin fluctuations. A sharp peak in electronic density of states below the Fermi level tends to render a negative fourth-order coefficient of the free energy expansion and an IEM is expected as demonstrated in many rare-earth and transition-metal compounds [9].

Among these compounds, $\text{LaFe}_{13-x}\text{Si}_x$ has attracted broad attention for its superior magnetocaloric performances [10,11]. With x in a very narrow doping range around 1.5, the system undergoes a sharp FM-PM FOMT at Curie temperature (T_C) of about 190 K, where there is a strong magnetoelastic coupling as reflected in a dramatic negative thermal expansion ($\Delta V/V \sim 1.5\%$, where V is the unit cell volume). Above T_C , a moderate magnetic field can induce a FOMT, giving rise to giant magnetic-entropy changes of about $-25 \text{ J kg}^{-1} \text{ K}^{-1}$. T_C of this system can be elevated up to 350 K by substituting Fe with Co atoms or by adding interstitial hydrogen atoms, which hardly reduces the magnetic-entropy changes [12,13]. For instance, $\text{La}(\text{Fe}_{0.94}\text{Co}_{0.06})_{11.9}\text{Si}_{1.1}$ has maximum magnetic-entropy changes of $-20 \text{ J kg}^{-1} \text{ K}^{-1}$ at $T_C \sim 280 \text{ K}$ [12]. Moreover, the thermal and magnetic hysteresis at the FOMT is small compared with other giant

*dyu@ansto.gov.au

†bingli@imr.ac.cn

‡fxhu@iphy.ac.cn

magnetocaloric materials [10]. In terms of real applications, $\text{LaFe}_{13-x}\text{Si}_x$ is also cost-effective given that it consists of earth-abundant elements.

Despite the outstanding magnetocaloric performances mentioned above that make this system promising for solid-state refrigeration applications, the exact mechanism of its FOMT remains unclear. A fundamental understanding of FOMT may foster the future designing of advanced magnetocaloric materials. IEM has been frequently used to account for the transition, but spin fluctuations themselves as the core of this mechanism have merely been investigated yet [14–16]. In recent neutron diffraction measurements, spin fluctuations arising from PM correlations were discovered above T_C [17]. In addition, nuclear resonant inelastic x-ray scattering shows partial phonon density of state (PDOS) of Fe sublattices is renormalized across T_C in $\text{LaFe}_{11.5}\text{Si}_{1.5}$ [18]. Thus spin-phonon coupling is believed to play a critical role in this system [18]. To thoroughly clarify the FOMT, it is necessary to conduct research considering lattice and magnetic degrees of freedom in both static and dynamic respects. Here, we present an investigation comparing $\text{LaFe}_{11.6}\text{Si}_{1.4}$ and $\text{LaFe}_{11.2}\text{Si}_{1.8}$, which exhibit a FOMT and a second-order magnetic transition (SOMT), respectively. Based on the complete lattice and spin dynamics, we are able to establish the differences between the two materials, and pinpoint the intense FM fluctuations as the decisive factor in the FOMT and hence in the giant magnetocaloric effect.

II. EXPERIMENTAL DETAILS

Polycrystalline $\text{LaFe}_{11.6}\text{Si}_{1.4}$ and $\text{LaFe}_{11.2}\text{Si}_{1.8}$ were prepared using an arc-melting method followed by a long time annealing to reduce the impurity phase of α -Fe, as previously described [10]. The obtained materials for the present study were of single phase without Fe impurity identified in laboratory x-ray diffraction measurements. Magnetization measurements were performed on a superconducting quantum interference device magnetometer (Quantum Design MPMS XL) to determine the transition temperatures, as shown in Supplemental Material Fig. S1 [19]. In terms of the temperature dependencies of magnetization at 100 Oe, T_C for $\text{LaFe}_{11.6}\text{Si}_{1.4}$ and $\text{LaFe}_{11.2}\text{Si}_{1.8}$ are determined to be 184 and 208 K, respectively.

The neutron scattering experiments were conducted on the time-of-flight neutron spectrometer Pelican at ANSTO [20]. The instrument was configured for incident neutron energy of 3.7 meV, with an energy resolution of 0.135 meV at the elastic line. The powder samples of $\text{LaFe}_{11.6}\text{Si}_{1.4}$ and $\text{LaFe}_{11.2}\text{Si}_{1.8}$ were loaded into an annular aluminum can with a sample thickness of 1 mm. The experiments were performed at 100, 160, 210, 250, 275, and 300 K for $\text{LaFe}_{11.6}\text{Si}_{1.4}$ and 100, 180, 250, 282, 300, and 340 K for $\text{LaFe}_{11.2}\text{Si}_{1.8}$. A background spectrum from an empty can was collected under the same conditions as the sample measurements. The instrument resolution function was measured on a standard vanadium can at 300 K. The spectrum of the vanadium standard was also used for detector normalization. All data reduction and manipulation, including background subtraction and detector normalization, were done using the large array manipulation program (LAMP) [21]. The scattering function $S(Q, E)$, which

is a function of scattering wave vectors (Q) and energy transfer (E), were measured on energy gain mode over a wide temperature range. And the scattering function $S(Q, E)$ transformed to a generalized PDOS by the formula (1), where k_B is the Boltzmann constant and T is the temperature [22],

$$g(E) = \int \frac{E}{Q^2} S(Q, E) (1 - e^{-E/k_B T}) dQ. \quad (1)$$

The constant- Q data were fitted with the PAN module in date analysis and visualization environment (DAVE) [23].

III. RESULTS AND DISCUSSION

$\text{LaFe}_{13-x}\text{Si}_x$ intermetallics crystallize in the cubic NaZn_{13} -type structure with space group $Fm\bar{3}c$ [10]. As shown in Fig. 1(a), the crystal structure appears as a cage configuration consisting of Fe atoms in which La atoms are trapped. There are two inequivalent crystallographic sites for Fe, i.e., Fe(I) on the 8-fold ($8b$) and Fe(II) on the 96-fold ($96i$) Wyckoff positions. The Fe(II) site is shared with Si. $\text{LaFe}_{11.6}\text{Si}_{1.4}$ has a FOMT at 184 K, while a SOMT occurs in $\text{LaFe}_{11.2}\text{Si}_{1.8}$ at 208 K (see Fig. S1 for their temperature dependencies of magnetization [19]). Given that the crystal structure is the same, the selected compositions are an ideal playground for understanding the lattice and spin dynamics.

Shown in Figs. 1(b) and 1(c) are PDOS for these two compositions in the vicinity of transitions up to 60 meV. The profiles of PDOS of the two compositions both feature a broad peak located at about 24 meV with a few small local maxima superimposed, in agreement with the previous report [18]. The profiles are essentially dominated by the partial PDOS from the Fe atoms as determined in nuclear resonant inelastic x-ray scattering measurements [18]. The overall line shapes do not change significantly across T_C , except for the shift to lower energies upon becoming PM. To quantitatively characterize the phonon softening at the transitions, we track the peak at 24 meV as a function of temperature. As plotted in Fig. 1(d), both compositions display remarkable softening. The observed softening here is unusual given that larger volumes of unit cells lead to reduced frequencies of phonon modes in an atomic system, whereas the FM phases of both compounds are considerably expanded. Such an exception just reflects the magnetic contribution to the phase transition. The decreases of energy at heating from 100 to 300 K are similar for both, but the change of $\text{LaFe}_{11.6}\text{Si}_{1.4}$ is slightly sharper, consistent with its nature of FOMT. Obviously, the magnetic softening of phonons across T_C are not unique to FOMT, but also for SOMT. Similar phonon softening is actually consistent with the fact that both compounds exhibit significant negative thermal expansions at the transitions as a consequence of magnetovolume effect. The similar spin-phonon coupling strength implies the minuteness of the lattice degree of freedom in this system. In this sense, phonon softening is impossible to solely account for differences between these two compositions. As such, in addition to phonons, we also examine the magnons. The FM states of both compositions show almost identical spin excitations below T_C . At 100 K, for example, strong spin excitations develop from the first Bragg peak, (200), and persist up to about 2 meV (Fig. S2 [19]).

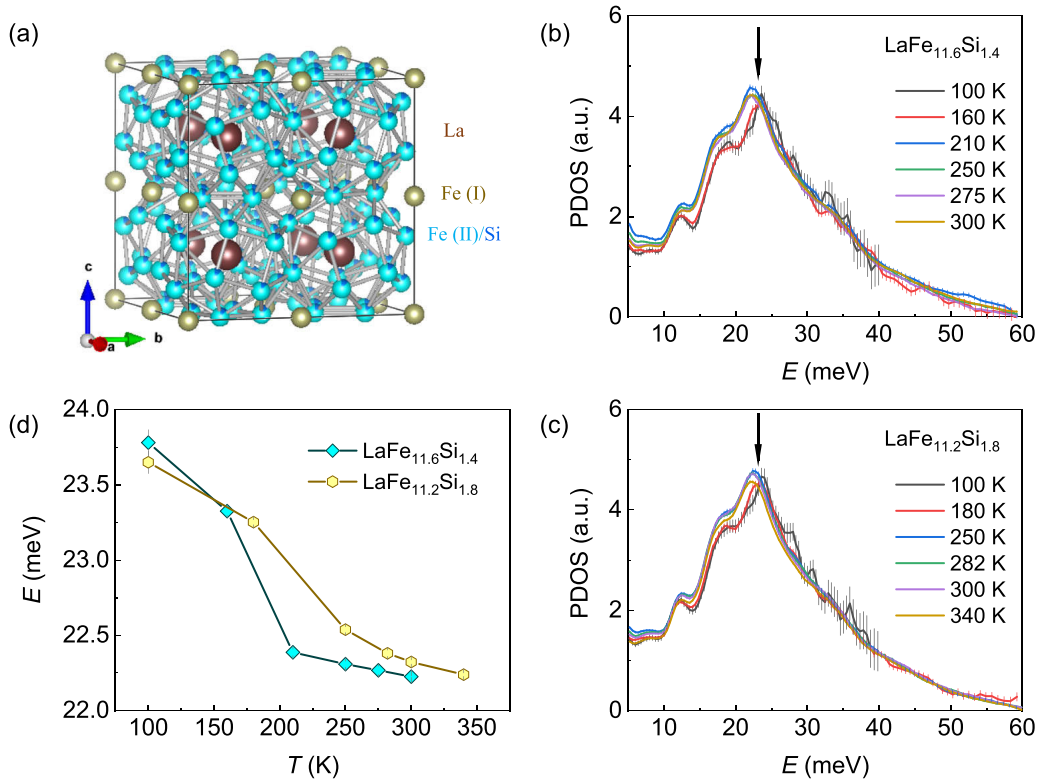


FIG. 1. Crystal structure and PDOS. (a) Crystal structure of the $\text{LaFe}_{13-x}\text{Si}_x$ system. (b),(c) PDOS of $\text{LaFe}_{11.6}\text{Si}_{1.4}$ and $\text{LaFe}_{11.2}\text{Si}_{1.8}$ at selected temperature across the phase transitions. The peak positions at about 24 meV are pointed out by arrows. (d) Temperature dependencies of the peak positions arrowed in (b) and (c).

Hereafter, we turn our attention to the PM states where spin fluctuations are expected. In Fig. 2(a), we plot the dynamic structure factor $S(Q, E)$ as a function of momentum transfer

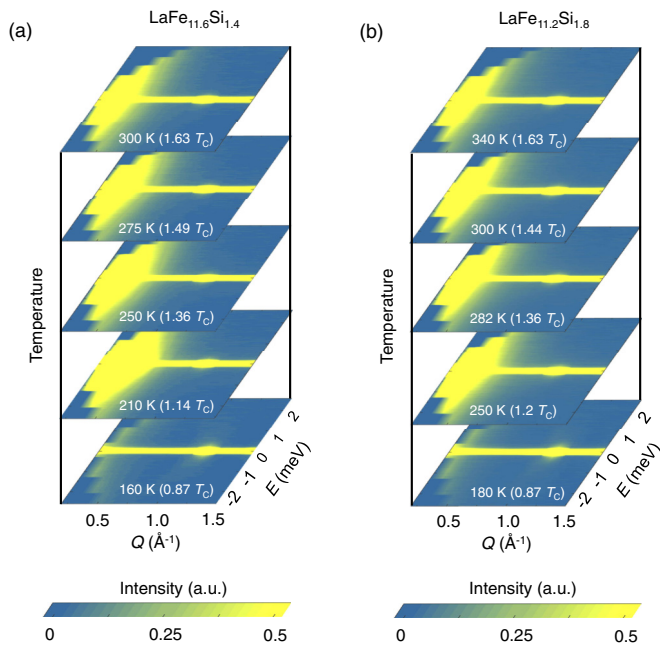


FIG. 2. Contour plots of magnetic diffuse scattering. Dynamic structure factor $S(Q, E)$ of $\text{LaFe}_{11.6}\text{Si}_{1.4}$ (a) and $\text{LaFe}_{11.2}\text{Si}_{1.8}$ (b) at different temperatures.

(Q) and energy transfer (E) at selected temperatures near T_C . In $\text{LaFe}_{11.6}\text{Si}_{1.4}$, at 210 K just above T_C , intense diffuse scattering is observed in the low- Q region. The intensity becomes weaker as the temperature rises from 210 to 300 K, but pronounced diffuse scattering is still detected at 300 K. In $\text{LaFe}_{11.2}\text{Si}_{1.8}$, similar diffuse scattering is found, as shown in Fig. 2(b). However, the intensity of magnetic diffuse scattering of $\text{LaFe}_{11.6}\text{Si}_{1.4}$ is obviously stronger. For instance, at the given color scales, the diffuse scattering of $\text{LaFe}_{11.6}\text{Si}_{1.4}$ at $1.36 T_C$ is extended up to $Q \sim 0.75 \text{ \AA}^{-1}$, whereas that of $\text{LaFe}_{11.2}\text{Si}_{1.8}$ decays at $Q \sim 0.6 \text{ \AA}^{-1}$.

In a search for exact differences between them, we exclude the elastic intensity by integrating the spectra in the intervals of $-2.55 \leq E \leq -0.15$ and $0.15 \leq E \leq 2.55 \text{ meV}$ at about $1.2 T_C$, as plotted in Fig. 3(a), given that the experimental energy resolution is about 0.135 meV. The obtained intensity of both compositions rapidly grows as Q decreases when $Q < 0.8 \text{ \AA}^{-1}$, typical of PM scattering [24]. Strikingly, an extra intensity is found between 0.4 and 0.8 \AA^{-1} for $\text{LaFe}_{11.6}\text{Si}_{1.4}$. The inset highlights their difference that peaks at about 0.5 \AA^{-1} . This position is close to the (100) Bragg peak ($Q \sim 0.54 \text{ \AA}^{-1}$), which is crystallographically forbidden. As the extra magnetic scattering intensity is peaked at 0.5 \AA^{-1} , detailed constant- Q spectra are investigated at different temperatures for $\text{LaFe}_{11.6}\text{Si}_{1.4}$ [Fig. 3(b)] as well as for $\text{LaFe}_{11.2}\text{Si}_{1.8}$ [Fig. 3(c)]. Below T_C , the spectra exhibit strong elastic peaks. Just above T_C , quasielastic neutron scattering (QENS) components are superimposed underneath the elastic peaks. As the temperature continues to rise, the QENS

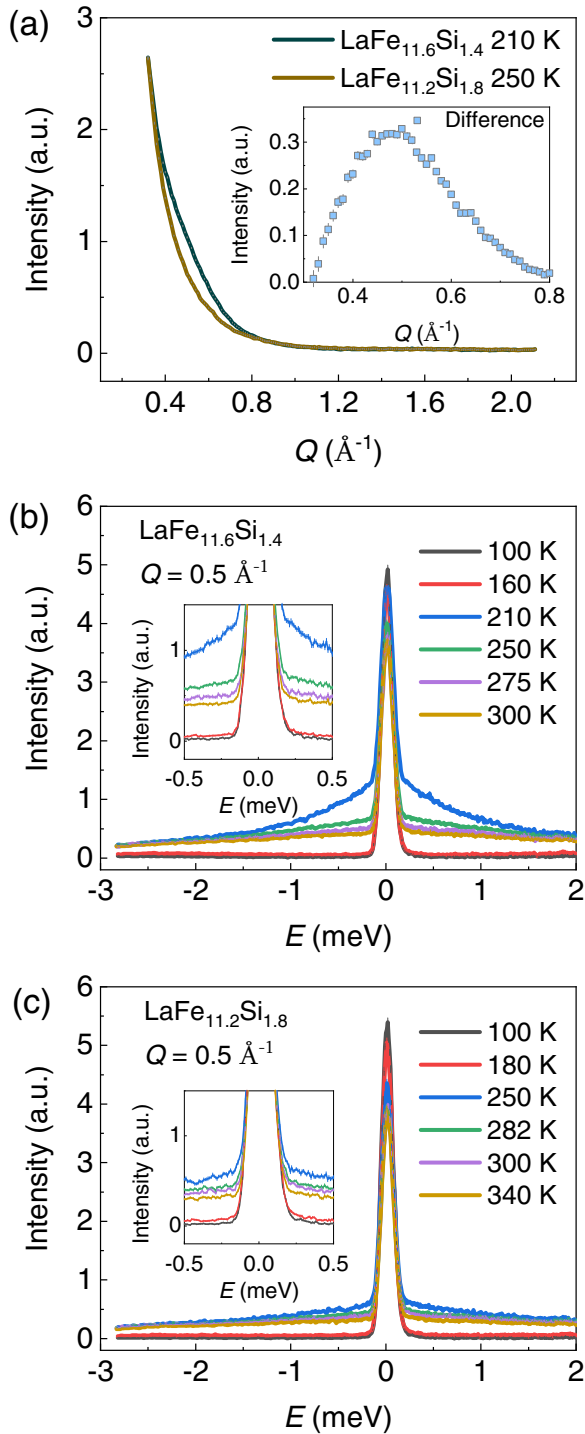


FIG. 3. Q dependence of magnetic diffuse scattering. (a) Intensity integrated at $-2.55 \leq E \leq -0.15$ meV and $0.15 \leq E \leq 2.6$ meV for $\text{LaFe}_{11.6}\text{Si}_{1.4}$ at 210 K and for $\text{LaFe}_{11.2}\text{Si}_{1.8}$ at 250 K. The inset shows their difference. (b),(c) QENS spectra at $Q = 0.5 \text{ \AA}^{-1}$ at different temperatures for $\text{LaFe}_{11.6}\text{Si}_{1.4}$ and $\text{LaFe}_{11.2}\text{Si}_{1.8}$. The insets highlight the low- E regions.

components become broader and weaker. Even so, it is still visible at $1.6T_C$. However, it is apparent that $\text{LaFe}_{11.6}\text{Si}_{1.4}$ exhibits much stronger QENS intensity at a same reduced temperature. Also, the QENS components in $\text{LaFe}_{11.6}\text{Si}_{1.4}$ are

more temperature dependent as the intensity is significantly suppressed when the temperature is changed from 210 to 250 K.

Henceforward, spectral fitting is used to extract accurate information on spin dynamics from the QENS intensity. At 210 K for $\text{LaFe}_{11.6}\text{Si}_{1.4}$, the spectrum at 0.5 \AA^{-1} is well reproduced by a combination of a delta function and two Lorentzian functions, which are all convoluted to the instrument resolution function [see Fig. 4(a)]. The delta function represents the elastic scattering while the Lorentzian function accounts for the dynamic diffuse scattering containing information on dynamic spin correlations with finite timescales. The wider spectrum, the faster spin fluctuations exist. This fitting yields a full width at half maximum (Γ) of 5.237 and 1.152 meV, which are compared to 5.613 and 1.538 meV at 250 K, respectively. As shown in Fig. 4(b), a similar fitting is applied to the spectrum of $\text{LaFe}_{11.2}\text{Si}_{1.8}$ at 250 K, which gives rise to Γ of 6.309 and 1.099 meV, respectively. Except for the three spectra mentioned above, others can be well reproduced by a combination of a delta function and one single Lorentzian function. As shown in Fig. S3 [19], the narrower one disappears with the wider one remaining. The temperature- and Q -dependent fitting results are summarized in Fig. S4 [19].

Based on the precise separation of scattering intensity presented above, we sum up the intensity of elastic scattering and the wider QENS component for $\text{LaFe}_{11.6}\text{Si}_{1.4}$ at 210 and 250 K as well as for $\text{LaFe}_{11.2}\text{Si}_{1.8}$ at 250 K, respectively, while all components for spectra at other temperatures are used. The results are plotted as a function of Q , which are fitted to equation $S(Q) = M(0)^2 \frac{(1/\xi_{PM})^2}{(1/\xi_{PM})^2 + Q^2}$ to obtain the PM correlation length (ξ_{PM}), where $M(0)^2$ is the static susceptibility in units of μ_B^2 [25]. Two examples are shown in Fig. 4(c). Similar fitting is applied to the data at other temperatures and the obtained temperature dependence of ξ_{PM} is summarized in Fig. 4(d). As the nearest neighboring Fe-Fe distance is about 2.5 \AA in this system, the obtained ξ_{PM} suggests that magnetic correlations are localized around the nearest neighboring Fe atoms at $1.6T_C$. At a given reduced temperature, it is evident that $\text{LaFe}_{11.6}\text{Si}_{1.4}$ has a slightly smaller ξ_{PM} than $\text{LaFe}_{11.2}\text{Si}_{1.8}$.

Unlike the PM scattering diverging towards lower Q , the intensity of the narrower Lorentzian function shows a well-defined peak at $Q \sim 0.5 \text{ \AA}^{-1}$, as shown in Figs. 4(e) and 4(f). This position is close to the crystallographically forbidden Bragg peak (100) and the $Q \sim 0.5 \text{ \AA}^{-1}$ peak represents ultrafast FM fluctuations [26]. This peak is fitted to a Gaussian function, yielding FM correlation length (ξ_{PM}) of 12.2 and 21.0 \AA , respectively. It is noted that the FM fluctuations are more remarkable in $\text{LaFe}_{11.6}\text{Si}_{1.4}$ as compared in Figs. 4(e) and 4(f). Moreover, at $1.35T_C$ the FM fluctuations are robust in $\text{LaFe}_{11.6}\text{Si}_{1.4}$ (at 250 K) whereas those become undetectable in $\text{LaFe}_{11.2}\text{Si}_{1.8}$ (at 282 K) within the present experimental resolution. As a result, the extra intensity shown in Fig. 3(a) turns out to originate from FM fluctuations. Here, we emphasize the uniqueness of the FM fluctuations observed here, compared to the common critical magnetic scattering. Just above magnetic ordering temperatures, magnetic diffuse scattering is often observed to be centered at positions of magnetic Bragg peaks and appears as a QENS signal imposed underneath the elastic scattering [27]. The spectral weight

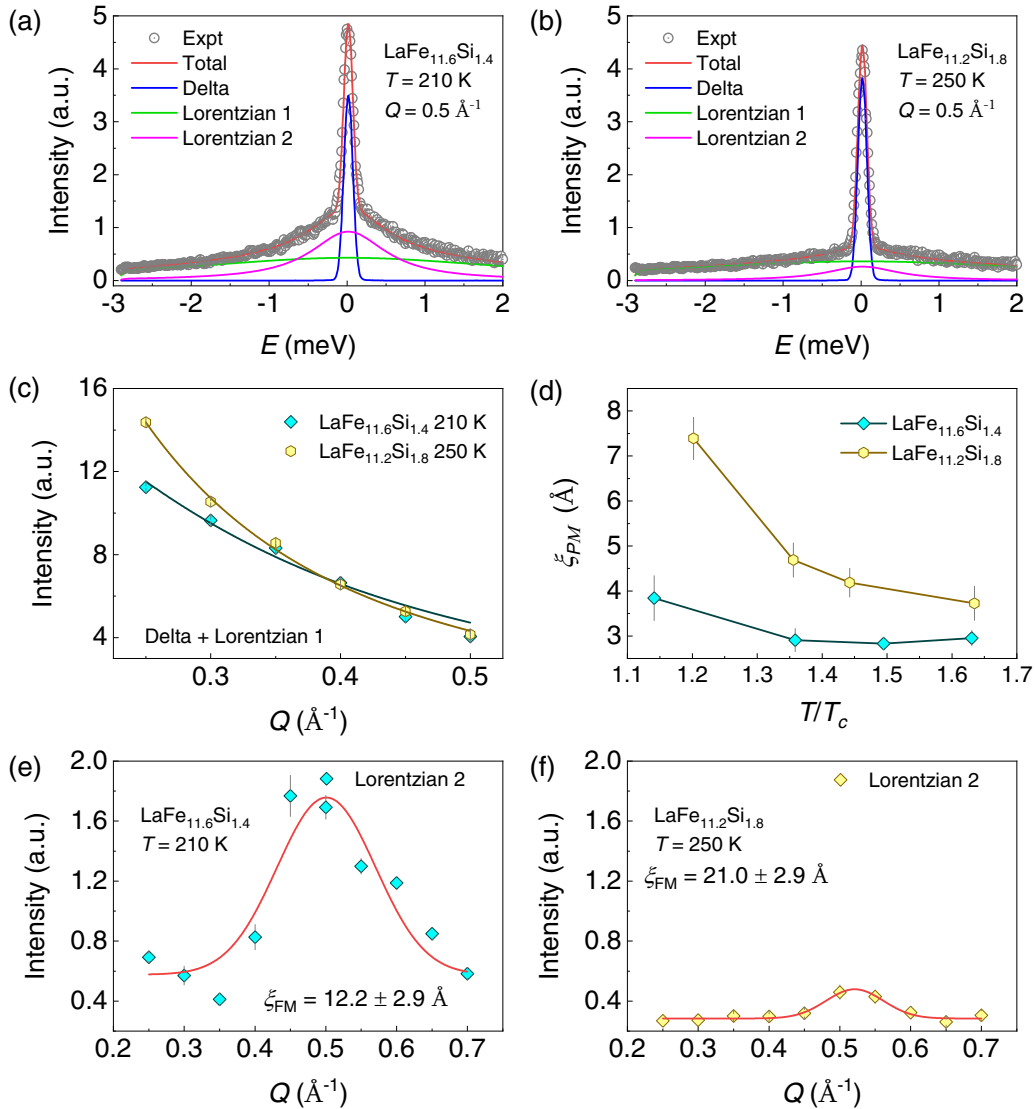


FIG. 4. Intense FM fluctuations. (a),(b) Spectral fitting at $Q = 0.5 \text{ \AA}^{-1}$ for $\text{LaFe}_{11.6}\text{Si}_{1.4}$ at 210 and $\text{LaFe}_{11.2}\text{Si}_{1.8}$ at 250 K. Each component is highlighted. (c) Q dependencies of intensity for $\text{LaFe}_{11.6}\text{Si}_{1.4}$ at 210 K and $\text{LaFe}_{11.2}\text{Si}_{1.8}$ at 250 K (Delta plus Lorentzian 1). The lines represent the fitting described in the main text. (d) PM correlation length (ξ_{PM}) determined by fitting as shown in (c). (e),(f) Q dependencies of the intensity of the Lorentzian 2 components for $\text{LaFe}_{11.6}\text{Si}_{1.4}$ at 210 K and $\text{LaFe}_{11.2}\text{Si}_{1.8}$ at 250 K. The lines represent the fitting to Gaussian functions yielding the FM correlation length (ξ_{FM}) as labeled.

of diffuse scattering is transferred to magnetic Bragg peaks and spin-wave excitations when the systems are magnetically ordered. In contrast, the FM fluctuations are only found in the position of Bragg peak (100). It can be seen in Fig. S5 [19] that the spectra at (200), the first Bragg peak in this system, are dominated by ordinary elastic peaks.

The spin dynamics are established above and the FOMT is revealed to be electronic in nature through FM fluctuations. It has been known for several decades that a first-order phase transition occurs when fluctuations are strong enough [28,29]. Recently, fluctuation-induced first-order phase transitions are widely observed in several different systems, like helimagnet MnSi [30] as well as frustrated antiferromagnets $\text{Gd}_2\text{Sn}_2\text{O}_7$ [31] and Mn_5Si_3 [32]. Hence, magnetic fluctuations might be a universal driving force of FOMTs. More specifically, we point out that the obtained conclusion is probably applicable

to similar magnetocaloric systems that exhibit FOMTs, like the $(\text{Mn, Fe})_2\text{AsP}$ system [33,34].

IV. SUMMARY

In summary, we have studied the $\text{LaFe}_{13-x}\text{Si}_x$ system using inelastic neutron scattering. The comparative study on $\text{LaFe}_{11.6}\text{Si}_{1.4}$ and $\text{LaFe}_{11.2}\text{Si}_{1.8}$ suggests the spin-phonon coupling is not unique to the FOMT and a similar phonon softening behavior at the PM to FM transitions regardless of the order of phase transitions, which might be related to the magnetovolume effects. Thus, the lattice degree of freedom is not able to account for the origin of the FOMT in this system. Instead, the FOMT manifests itself as much stronger FM spin fluctuations in the PM state. The findings in this model system demonstrate that a universal scenario might be established

based on robust FM fluctuations for FOMTs, which are the central issue of giant magnetocaloric materials.

ACKNOWLEDGMENTS

The work conducted at the Institute of Metal Research was supported by the Ministry of Science and Technology of China (Grant No. 2020YFA0406001), the Key Research Program of Frontier Sciences of Chinese Academy of Sciences (Grant No. ZDBS-LY-JSC002), the Liaoning Revitalization

Talents Program (Grant No. XLYC1807122), and National Natural Science Foundation of China (Grant No. 51771197). The work conducted at the Institute of Physics was supported by the Ministry of Science and Technology of China (Grant No. 2019YFA0704900) and the National Natural Science Foundation of China (Grant No. U1832219). The authors acknowledge beam time awarded by ANSTO (Proposal No. P7867) and Yanna Chen, Yue Cao, J. S. Gardner, and E. Brück for the discussion.

The authors declare no conflict of interest.

-
- [1] M. Imada, A. Fujimori, and Y. Tokura, *Rev. Mod. Phys.* **70**, 1039 (1998).
- [2] H. Kuwahara, Y. Tomioka, A. Asamitsu, Y. Moritomo, and Y. Tokura, *Science* **270**, 961 (1995).
- [3] A. Asamitsu, Y. Tomioka, H. Kuwahara, and T. Tokura, *Nature (London)* **388**, 50 (1997).
- [4] V. K. Pecharsky and K. A. Gschneidner, Jr., *Phys. Rev. Lett.* **78**, 4494 (1997).
- [5] R. Kainuma, Y. Imano, W. Ito, Y. Sutou, H. Morito, S. Okamoto, O. Kitakami, K. Oikawa, A. Fujita, T. Kanomata, and K. Ishida, *Nature (London)* **439**, 957 (2006).
- [6] F. Guillou, A. K. Pathak, D. Paudyal, Y. Mudryk, F. Wilhelm, A. Rogalev, and V. K. Pecharsky, *Nat. Commun.* **9**, 2925 (2018).
- [7] J. Łażewski, P. Piekarczyk, J. Toboła, B. Wiendlocha, P. T. Jochym, M. Sternik, and K. Parlinski, *Phys. Rev. Lett.* **104**, 147205 (2010).
- [8] J. Liu, T. Gottschall, K. P. Skokov, J. D. Moore, and O. Gutfleisch, *Nat. Mater.* **11**, 620 (2012).
- [9] K. Fukamichi, *Itinerant-Electron Metamagnetism, Handbook of Advanced Magnetic Materials* (Springer, Berlin, 2006).
- [10] B. Shen, J. Sun, F. Hu, H. Zhang, and Z. Cheng, *Adv. Mater.* **21**, 4545 (2009).
- [11] F. Hu, B. Shen, J. Sun, Z. Cheng, G. Rao, and X. Zhang, *Appl. Phys. Lett.* **78**, 3675 (2001).
- [12] F. Hu, J. Gao, X. Qian, M. Ilyn, A. M. Tishin, J. Sun, and B. Shen, *J. Appl. Phys.* **97**, 10M303 (2005).
- [13] A. Fujita, S. Fujieda, Y. Hasegawa, and K. Fukamichi, *Phys. Rev. B* **67**, 104416 (2003).
- [14] A. Fujita, K. Fukamichi, J.-T. Wang, and Y. Kawazoe, *Phys. Rev. B* **68**, 104431 (2003).
- [15] A. Fujita, S. Fujieda, K. Fukamichi, H. Mitamura, and T. Goto, *Phys. Rev. B* **65**, 014410 (2001).
- [16] M. E. Gruner, W. Keune, J. Landers, S. Salamon, M. Krautz, J. Zhao, M. Y. Hu, T. Toellner, E. E. Alp, O. Gutfleisch, and H. Wende, *Phys. Status Solidi B* **255**, 1700465 (2018).
- [17] T. Faske, I. A. Radulov, M. Hölzel, O. Gutfleisch, and W. Donner, *J. Phys.: Condens. Matter* **32**, 115802 (2020).
- [18] M. E. Gruner, W. Keune, B. Roldan Cuenya, C. Weis, J. Landers, S. I. Makarov, D. Klar, M. Y. Hu, E. E. Alp, J. Zhao, M. Krautz, O. Gutfleisch, and H. Wende, *Phys. Rev. Lett.* **114**, 057202 (2015).
- [19] See Supplemental Material at <http://link.aps.org/supplemental/10.1103/PhysRevMaterials.5.L071401> for the sample information and additional neutron scattering data.
- [20] D. Yu, R. Mole, T. Noakes, S. Kennedy, and R. Robinson, *J. Phys. Soc. Jpn.* **82**, SA027 (2013).
- [21] D. Richard, M. Ferrand, and G. J. Kearley, *J. Neutron Res.* **4**, 33 (1996).
- [22] A. Furrer, J. Mesot, and T. Strässle, *Neutron Scattering in Condensed Matter Physics* (World Scientific Publishing Co. Pte. Ltd., Singapore, 2009).
- [23] R. T. Azaiah, L. R. Kneller, Y. Qiu, P. L. W. Tregenna-Piggott, C. M. Brown, J. R. D. Copley, and R. M. Dimeo, *J. Res. Natl. Inst. Stand. Technol.* **114**, 341 (2009).
- [24] J. Hubbard, *J. Appl. Phys.* **42**, 1390 (1971).
- [25] P. J. Brown, H. Capellman, J. Déportes, D. Givord, S. M. Johnson, and K. R. A. Ziebeck, *J. Phys.* **47**, 491 (1986).
- [26] A. T. Boothroyd, R. Coldea, D. A. Tennant, D. Prabhakaran, L. M. Helme, and C. D. Frost, *Phys. Rev. Lett.* **92**, 197201 (2004).
- [27] T. Chatterji, *Paramagnetic and Critical Scattering, Neutron Scattering from Magnetic Materials* (Elsevier Science, Amsterdam, 2006).
- [28] S. A. Brazovskii, I. E. Dzyaloshinskii, and B. G. Kukhareno, *Zh. Eksp. Teor. Fiz.* **70**, 2257 (1976) [*Sov. Phys. JETP* **43**, 1178 (1976)].
- [29] K. G. Wilson, *Rev. Mod. Phys.* **55**, 583 (1983).
- [30] M. Janoschek, M. Garst, A. Bauer, P. Krautscheid, R. Georgii, P. Böni, and C. Pfleiderer, *Phys. Rev. B* **87**, 134407 (2013).
- [31] O. Cépas, A. P. Young, and B. S. Shastry, *Phys. Rev. B* **72**, 184408 (2005).
- [32] N. Biniskos, K. Schmalzl, S. Raymond, S. Petit, P. Steffens, J. Persson, and T. Brückel, *Phys. Rev. Lett.* **120**, 257205 (2018).
- [33] X. F. Miao, L. Caron, J. Cedervall, P. C. M. Gubbens, P. Dalmás de Réotier, A. Yaouanc, F. Qian, A. R. Wildes, H. Luetkens, A. Amato, N. H. van Dijk, and E. Brück, *Phys. Rev. B* **94**, 014426 (2016).
- [34] H. Fujii, Y. Uwatoko, K. Motoya, Y. Ito, and T. Okamoto, *J. Phys. Soc. Jpn.* **57**, 2143 (1988).